Liquid-Crystalline Suspensions of Photosensitive Paramagnetic CeF 3 Nanodiscs

Fréderic Chaput, Frédéric Lerouge, Anne-Laure L Bulin, David Amans, Mateusz Odziomek, Anne-Charlotte C Faure, Maelle Monteil, Ivan Dozov, Stéphane Parola, Frédéric Bouquet, et al.

Liquid-crystalline suspensions of photosensitive paramagnetic CeF_3 nanodiscs

Frédéric Chaput[a], Frédéric Lerouge[a], Anne-Laure Bulin[b], David Amans[b], Odziomek Mateusz[a], Anne-Charlotte Faure[a], Maelle Monteil[c], Ivan Dozov[d], Stéphane Parola[a], Frédéric Bouquet[d], Marc Lecouvey[c], Patrick Davidson[d]* and Christophe Dujardin[b]*

Dr. F. Chaput, Dr. F. Lerouge, Dr M. Odziomek, Dr. A.C. Faure and Prof. S. Parola
Université de Lyon, Ens de Lyon, CNRS UMR 5182, Université Claude Bernard Lyon 1, Laboratoire de Chimie, F69342, Lyon, France.
E-mail: frederic.lerouge@univ-lyon1.fr
Dr. A.L. Bulin, Dr. D. Amans and Prof. C. Dujardin
Univ Lyon, Université Claude Bernard Lyon 1, CNRS UMR 5306, Institut Lumière Matière, F-69622, VILLEURBANNE, France
Dr. M. Monteil and Prof. M. Lecouvey
Laboratoire CSPBAT, UMR 7244, CNRS, Université Paris 13, 74 Rue Marcel Cachin, 93017 Bobigny, France.
Dr. Ivan Dozov, Dr. Frédéric Bouquet and Dr. P. Davidson
Laboratoire de Physique des Solides, CNRS, Univ. Paris-Sud, Université Paris-Saclay, 91405 Orsay Cedex, France
E-mail: patrick.davidson@u-psud.fr

Keywords: Cerium fluoride, crystalline nanodiscs, liquid crystals, photosensitive materials.

Abstract text.

The design of high-performance energy-converting materials is an essential step for the development of sensors but the elaboration of the bulk materials currently used remains costly and difficult. Therefore, a different approach based on the self-assembly of nanoparticles has been explored. We report on the preparation by solvothermal synthesis of highly crystalline CeF_3 nanodiscs. Their surface modification by bisphosphonate ligands led to stable, highly concentrated, colloidal suspensions in water. Despite the low aspect ratio of the nanodiscs (~ 6), a liquid-crystalline nematic phase spontaneously appeared in these colloidal suspensions. Thanks to the paramagnetic character of the nanodiscs, the nematic phase was easily aligned by a weak (0.5 T) magnetic field, which provides a simple and convenient way of orienting all the nanodiscs in suspension in the same direction. Moreover, the more dilute, isotropic, suspensions displayed strong (electric and magnetic) field-induced orientation of the nanodiscs (Kerr and Cotton-Mouton effects), with fast enough response times to make them suitable for use in electro-optic devices. Furthermore, emission study showed a direct relation between fluorescence intensity and magnetic field induced orientation of the colloids. Finally, with their fast radiative recombination decay rates, the nanodiscs show luminescence properties that compare quite favourably with those of bulk CeF_3. Therefore, these CeF_3 nanodiscs are very promising building blocks for the development and processing of photosensitive materials for sensor applications.

Introduction

Photo responsive materials which transform highly energetic radiations into UV/Vis photons easily detectable by conventional detectors are important for various applications such as high energy physics,[1] medical imaging [2] and nuclear industry.[3] The most important features of such materials are the efficiency of energy conversion, the luminescence decay time, the density, and the physical and chemical stabilities.[4] Whatever their nature, the currently used systems

are limited by intrinsic drawbacks. On the one hand, inorganic crystals show outstanding properties but their use is limited by their high cost and their complicated elaboration or working conditions. For example, some of them must be prepared in high-temperature furnaces while others, based on high-purity germanium, must be operated at liquid-nitrogen temperature. On the other hand, energy converters based on polymeric materials are cheap and easy to manufacture but they exhibit a lower light yield and a lower density.[5] Therefore, the design of a new kind of photosensitive materials featuring the high performance of inorganic crystalline systems together with the low-cost preparation of organic materials remains a target of choice.

The elaboration of photoresponsive material from luminescent nanoparticles could be a solution to this problem. For this purpose, we developed a method for rare-earth fluoride nanoparticle preparation that produces highly-crystalline nano-objects and that can easily be scaled up.[6] A remaining issue inherent to this approach is the production of functional materials from nanoparticles, for example as thin films of large dimensions. This step could be achieved by dispersing nanoparticles in a solvent to obtain stable colloids that could be processed for large-scale applications, by spin-coating for instance.

In single-crystal form, CeF_3 is a well-known material that meets many of the required criteria, including even those for high-energy particle calorimetry.[7] CeF_3 exhibits a reasonable emission yield of ~ 4500 photons per MeV, a fast decay time of ~ 20 ns out of any slow component, and a density of 6.16 g/cm3, which makes it a photosensitive material of high interest. Moreover, CeF_3 nanoparticles are easily produced[8] and were recently described as potential nano-emitters for photodynamic therapy under ionizing radiation.[9]

Here, we report on the synthesis and characterization of cerium fluoride nanodiscs and on their functionalization with bisphosphonate ligands to disperse them in water. In spite of the low aspect ratio of these nanodiscs, we discovered that their colloidal aqueous suspensions exhibit a liquid-crystalline nematic phase. Moreover, since the nanoparticles are paramagnetic, the nematic phase is easily aligned in a small magnetic field. Furthermore, the isotropic phase also shows strong (magnetic and electric) field-induced-alignment effects. Interestingly, such magnetically induced alignment effect has a direct impact on the emission properties of the nanodiscs suspensions, with a strong decrease of the fluorescence intensity when submitted to the field. Finally, the nanodiscs in suspension display very good scintillating properties that compare quite favourably with those of CeF_3 bulk crystals.

Experimental Section

Synthesis of aqueous colloidal suspensions of CeF_3 nanodiscs: In a typical synthesis, 1.49 g (4 mmol.) of cerium (III) chloride heptahydrate ($CeCl_3.7H_2O$, Aldrich) was dissolved in 16 mL of methanol (Solution A). In parallel, 0.45 g (9 mmol.) of hydrofluoric acid (40 wt.% in H_2O, Aldrich) was mixed with 16 mL of N-Methyl-2-pyrrolidone (Solution B). Subsequently, solution A was added to solution B under vigorous stirring. After stirring for 15 min, the reaction medium was transferred into a Teflon-lined stainless-steel autoclave (Berghof, DAB-2, inner volume, 25 mL). The autoclave was sealed, heated to 170 °C, and kept at that temperature for 1 h. After cooling to room temperature, acetone was added to the suspension and the precipitate was collected by centrifugation. The supernatant was carefully removed and the precipitate was washed with methanol and centrifuged. This washing process was repeated twice. Finally, the precipitate was dispersed in water and PEG-functionalized bisphosphonate was added in the as-prepared colloidal suspension (Ce/P molar ratio = 6/1). The mixture was stirred at 50 °C for 1 h.

To remove excess bisphosphonate molecules, a purification step by dialysis was performed. After freezing the solution, the nanodiscs were recovered by freeze-drying. Colloidal suspensions of CeF_3 nanodiscs with known weight fraction were prepared by dispersing precisely weighed amounts of nanodisc powder in deionized water.

Nanoparticle Characterization: TEM was performed with a TOPCON 002B microscope operating at 200 kV. The inter-reticular distances were measured on the fast Fourier transforms of the HRTEM pictures, using the Digital Micrograph software from Gatan; samples were prepared on a 5 nm-thick carbon-coated copper grid. X-ray powder diffraction (XRD) experiments (Bruker, D8 Advance A25 diffractometer) were performed to characterize the samples prepared. FT-IR analysis of the samples was performed using a PerkinElmer Spectrum 100 FT-IR spectrometer equipped with an attenuated total reflectance (ATR) sample chamber.

Optical microscopy: Colloidal suspensions of CeF_3 nanodiscs were filled into VitroCom optical flat glass capillaries of thickness 0.2 mm and width 2 mm to perform magneto-optic and electro-optic experiments. Samples were observed between crossed polarizers with an Olympus BX51 microscope equipped with an Olympus XZ-1 camera. We used a magnetic field setup based on two small permanent magnets. To apply a magnetic field, the sample was placed in between the two magnets, and the intensity of the field could easily be tuned between 0 and 1 T by changing the distance between the magnets, as already described.[36] The magnetic-field-induced birefringence was measured with the help of an Olympus optical compensator. A high-frequency ($f = 500$ kHz) a.c. electric field was applied to the sample thanks to a home-made cell, already described, with aluminum electrodes located outside the capillary.[28] The electric-field-induced birefringence was measured with the help of a photomultiplier tube. The measurement technique was described in great detail in reference.[36]

Magnetization measurements: A Quantum Design MPMS Squid apparatus was used to measure the sample magnetization in the temperature range of 10 to 300 K and in fields up to 1 T. A mass of 29.3 mg CeF_3 nanoparticle powder was inserted into a standard gelatin capsule, whose contribution (about 6% of the total signal) was subtracted from the measurements. The contribution of the ligands to the total mass was neglected in front of that of the nanoparticles.

Small-angle x-ray scattering: SAXS experiments were done at the high-brilliance ID02 beamline of the European Synchrotron Radiation Facility in Grenoble, France. The X-ray energy was 12.48 keV and the sample-to-detector distance was 2.01 m, which leads to an accessible q-range of 0.1 – 1.5 nm^{-1} where q is the scattering vector modulus $q = (4\pi/\lambda)\sin\theta$, $\lambda = 0.0993$ nm is the X-ray wavelength, and 2θ is the scattering angle. The detector was a Frelon camera with pixel size of 24 μm. Samples were held in the same capillaries used for optical microscopy and were submitted to a 0.5 T magnetic field just before X-ray exposure.

Luminescence : Radioluminescence (RL) spectra measurements were obtained by irradiating the samples with a Philips X-ray tube with tungsten anode set at 30 kV and 30 mA at room temperature. The emitted light was collected via an optical fiber and detected by an Andor Newton 970 CCD camera coupled to a monochromator (Andor Shamrock 500i) working in the 200 - 1000 nm interval. Radioluminescence (RL) time decay of the samples was obtained with the Pico-X (voltage 30 kV, laser frequency 1 MHz), without using any filter in front of the photomultiplier.

Results and discussion

The nanodiscs were prepared by following a previously described approach,[6] although the synthesis was somewhat modified, as detailed in Figure 1. Briefly, a mixture of N-Methyl-2-

pyrrolidone (NMP) / hydrofluoric acid (HF) / cerium chloride and methanol was treated by solvothermal process leading to an off-white precipitate. The obtained nanoparticles were purified by precipitation / re-dispersion before functionalization in aqueous medium with bisphosphonate derivatives bearing a polyethylene glycol chain. After purification by dialysis, the nanoparticle suspension was freeze-dried. The resulting powder was used firstly to study the physicochemical properties of the nanoparticles, and secondly to prepare highly- concentrated aqueous colloidal dispersions.

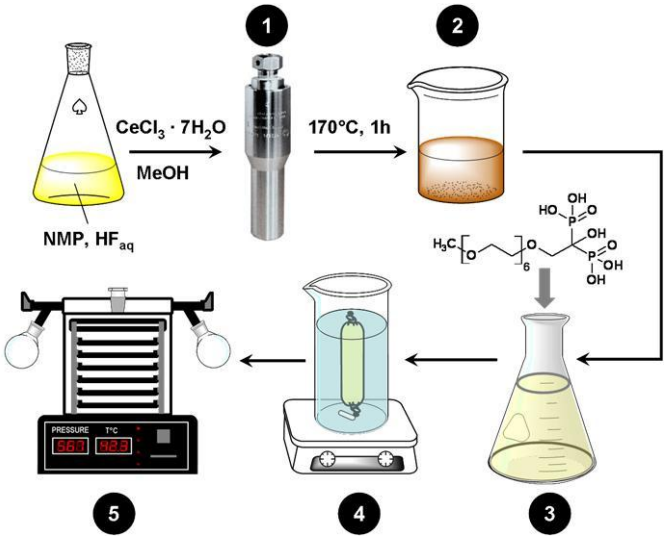

Figure 1. Process of elaboration and functionalization of CeF3 nanodiscs. Step 1: solvothermal treatment, step 2: precipitation in acetone, step 3: surface modification with bisphosphonates, step 4: purification by dialysis, and step 5: Freeze-drying.

Before functionalization with bisphosphonate ligands, the CeF_3 nanodiscs were analysed by transmission electron microscopy (TEM) and high-resolution TEM (HRTEM) measurements. Figure 2-a and b show the nanodiscs and the diameter distribution deduced from a statistical analysis performed over 214 particles. Only nanodiscs were observed but their diameter (D) distribution is quite broad, with 40 nm mean diameter and 32 nm standard deviation. We

managed to image some of the discs along their edge in order to evaluate their thickness (see Figures 2-c4 and S1-a). The thickness distribution was obtained from a set of 78 particles (see Figure S1-b). Unlike the broad diameter distribution, the thickness (t) distribution is sharp, with 6.7 nm mean thickness and 1.45 nm standard deviation. Figure S1-a demonstrates that there is no clear correlation between thickness and diameter.

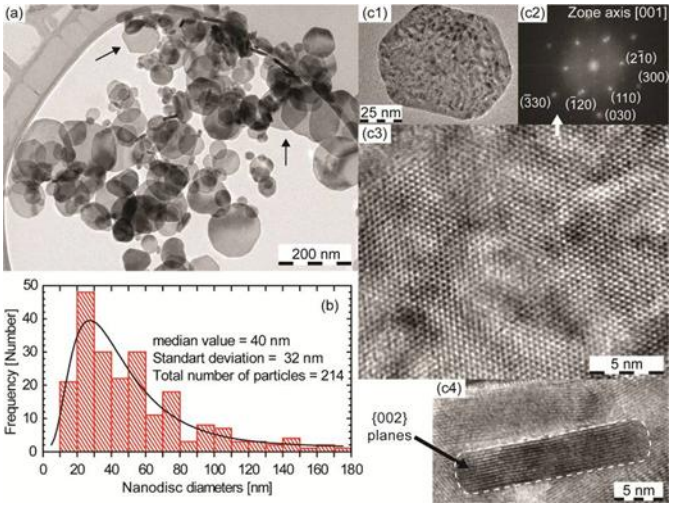

Figure 2. (a) Representative TEM picture at low magnification. Both arrows point to nanodiscs with hexagonal shape. (b) Size distribution of the nanodisc diameters. The size distribution is fitted with a log-normal law (black line). (c) Representative high-resolution images of CeF_3 nanodiscs crystallized in the P63/mcm space group, with its main axis (perpendicular to the basal plane) along the [001] crystal direction. (c1) Nanodisc with hexagonal shape. (c3) Details of an HRTEM picture and (c2) its corresponding Fast Fourier Transform. Image (c4) shows a disc upright on its edge. Consistently with Figure c3, the lattice plane family observed is {002}.

The HRTEM measurements show a mono-crystalline structure with no twin boundary (Figure 2c). The inter-reticular distances and their angles were analysed on 31 nanodiscs. Out of these, 30 nanodiscs gave an electronic diffraction pattern which fits the space group # 193 (Hexagonal system, space group P63/mcm) reported in the ICDD file 00-008-0045 (Fig. 2-c2). Only one

electronic diffraction pattern fits the space group # 139 (Tetragonal system, space group I4/mmm, ICCD file 04-013-3656). The XRD diagram (Figure S2) is consistent with the HRTEM results (P63/mcm) and no peak of any other phase or impurity was detected. Furthermore, the diagram exhibits both narrow ((300) for example) and broad ((111) and (113)) diffraction peaks, which is due to the anisotropic morphology of the nanoparticles. Finally, 28 nanodiscs (out of 30) have their main axis along the [001] crystalline direction. Therefore, the growth process seems to favor the (001) planes of the particles, orthogonal to the [001] direction, and the nanodiscs grow more along their rim than along their normal, which leads to their anisotropic shape.

After purification, the nanodiscs were functionalized with polyethylene glycol (PEG)-modified bisphosphonate as surface-capping molecule. It is indeed well known that bisphosphonates exhibit high affinity for metal oxide/hydroxide surfaces. However, very few articles report on the surface modification of lanthanide fluoride nanoparticles by bisphosphonate molecules.[10] The preparation method of the bisphosphonate is described in Supporting Information. The bisphosphonate ligand grafting efficiency was monitored by Fourier transform infrared spectroscopy (FT-IR) of the nanodiscs before and after functionalization (Figure 3).

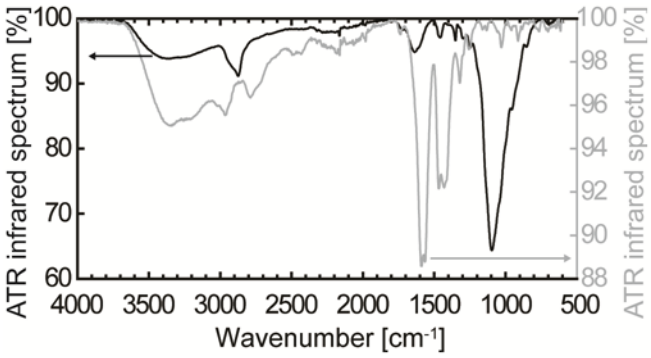

Figure 3. FTIR spectra of CeF_3 nanodiscs before (grey line) and after (dark line) bisphosphonate functionalization.

The FT-IR spectrum of the nanodiscs before grafting shows two strong peaks near 1590 and 1420 cm-1 which can be respectively assigned to COO- antisymmetric and symmetric stretching vibrations of carboxylate complexing surface cations. These carboxylate ligands are related to 4-(methylamino)butanoic acid produced by the NMP acidic hydrolysis at elevated temperature.[11] These two characteristic IR bands vary in position and shape depending on the coordination mode. According to Nakamoto, the frequency separation $\Delta\nu_{a\text{-}s}$ between the antisymmetric - ν_a (COO) - and the symmetric - ν_s (COO) - bands can be used to determine the interaction type between the carboxylate head and the metal ions.[12] In our study, the difference $\Delta\nu_{a\text{-}s}$ is equal to 165 cm-1, suggesting a coordination of carboxylate groups to metal ions in a bridging bidentate way. The formation of 4-(methylamino)butanoic acid at the surface of the nanodiscs is also associated with several other bands (3390 cm^{-1}: νNH; 2966 cm^{-1}: νCH_2 and νCH_3; 2770 cm^{-1}: R-NH-CH_3; 1471 cm^{-1}: νCH_2; 1320 cm^{-1}: νCH_3; 1137 cm^{-1}: νC-N). After functionalization with the bisphosphonate, the FT-IR spectrum confirms the surface modification of the CeF_3 nanoparticles. The carboxylate signature has almost disappeared while a strong absorption band can be observed at 1100 cm^{-1} that is characteristic of PO_3^{2-} vibration, indicating that the carboxylic acid has been replaced by bisphophonate ligands.

The dependence of the room-temperature magnetization on the magnetic-field intensity of the functionalized nanodiscs was measured up to 1 T. This dependence demonstrates the paramagnetic character of the particles, with a susceptibility χ(300 K) = 2.25×10-3 emu/mol (Figure 4 left part). Moreover, we measured the temperature dependence of χ(T) from 300 to 10

K, under a 0.1 T magnetic field, and found that χ follows the Curie-Weiss law $\chi(T) = C / (T - \theta)$ above 50 K, with C = 0.80 emu K / mol and θ = 53 K (Figure 4 right part). This behavior is very similar to that observed in bulk samples.[13]

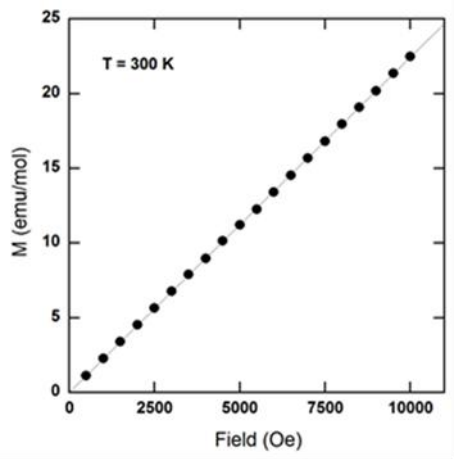

Figure 4. Squid measurements. Left part: Magnetic field dependence of the magnetization of CeF3 at room temperature. Right part: Temperature dependence of the inverse magnetic susceptibility of CeF3, measured under 1000 Oe. The straight line represents a Curie-Weiss fit $\chi(T) = C / (T - \theta)$ of the data above 50 K, with C = 0.80 emu K/mol and θ = 53 K.

Thanks to their functionalization by bisphosphonate ligands, the CeF_3 nanodiscs can easily be dispersed in deionized water up to very high weight fractions, leading to concentrated aqueous colloidal suspensions. The phase behaviour of these dispersions was investigated upon increasing concentration by visual inspection and optical microscopy in both natural and polarized light.

Below 30 wt%, the colloidal dispersions show no contrast by optical microscopy and look completely dark between crossed polarizers (data not shown). Hence, they are usual isotropic liquids with no organization of the nanodiscs. In spite of the small particle dimensions, the suspensions strongly scatter light due to the high concentration and the large contrast in optical

index between CeF_3 (n ~ 1.6) and the aqueous solvent (n = 1.33). Moreover, a small density gradient appeared in capillaries stored vertically for months, which is probably due to a weak aggregation occurring at such high concentrations.

At 30 wt%, the suspensions in optical capillaries, stored vertically for several weeks, spontaneously demixed in a very small amount of a birefringent nematic (N) phase, visible at the bottom of the capillaries, coexisting with a very large amount of the isotropic (I) phase at the top (Figure 5). In contrast with the usual isotropic phase, in the nematic phase, the nanodiscs align in the same direction (within each nematic domain). The isotropic/nematic phase separation proceeds through the nucleation in the bulk of small nematic droplets, called tactoids, that slowly sediment to the bottom of the capillary and coalesce to form the nematic phase (Figure S3).[14]

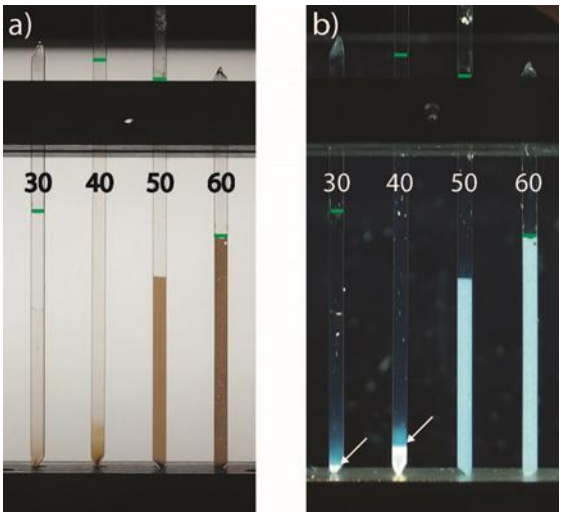

Figure 5. Flat capillaries (2 mm wide) filled with aqueous colloidal suspensions of CeF_3 nanodiscs of 30, 40, 50, and 60 % weight fraction observed with the naked eye a) in natural light and b) between crossed polarizers. The small green bars represent the suspension/air meniscus (i.e. the total suspension height) and the small white arrows point at the I/N interface.

These simple observations demonstrate the existence of a thermodynamic I/N 1st order phase transition.[15] Moreover, close examination of the nematic phase in polarized-light microscopy reveals large homeotropic domains (i.e. with the nanodiscs lying parallel to the flat faces of the optical capillary), and also typical schlieren textures (Figures 6 and S3).[16]

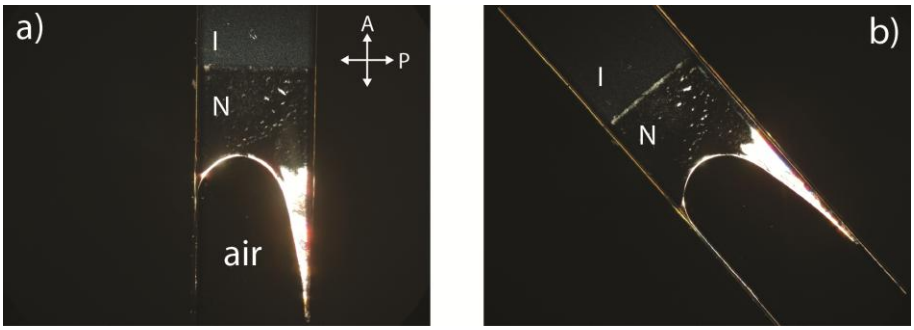

Figure 6. Textures in polarized-light microscopy of a 30 wt% sample showing the isotropic/nematic (I/N) phase coexistence. (An air bubble lies at the bottom of the capillary.) Capillary axis a) parallel to and b) at 45 degrees from the analyzer direction. The nematic phase looks mostly dark between crossed polarizers (white arrows) because it is homeotropically aligned on the flat faces of the capillary, except at the I/N and N/air meniscuses where it is planar and therefore quite bright.

At 40 wt%, the suspensions still display the I/N phase coexistence (Figure 5) but the proportion of nematic phase is larger, as expected. The observation of a nematic phase in suspensions of nanoparticles of rather low aspect ratio, D/t ~ 6, is actually remarkable. Indeed, nematic phases were so far mostly reported for much more anisotropic particles of aspect ratios ranging from ~ 12 for gibbsite and $Ni(OH)_2$ platelets[17] to ~ 1000 for clay, niobates, and graphene nanosheets.[18] Nevertheless, numerical simulations of hard discs predict that both the nematic and columnar phases can be stable for aspect ratios as low as respectively ~ 6 and ~ 4, albeit at

very large concentrations. [19] Therefore, our observation of the nematic phase confirms these simulations. However, in our experiments, we did not detect the columnar phase, in which the discs stack in columns assembled on a 2-dimensional (2D) lattice. This is most probably due to the polydispersity in diameter of the particles which is known to destabilize this phase with long-range 2-D positional order.[20]

Capillaries filled with dispersions at 50 wt% concentration also show phase coexistence (Figure 5) but the phases are very different from those described above. The bottom phase is an amorphous sediment which is little birefringent but strongly scatters depolarized light. This gel-like sediment expels a large amount of solvent (top phase) by syneresis. There is no sign left of the fluid nematic phase observed at lower concentration, which means that the upper concentration limit of the I/N biphasic region cannot be reached in this system because of the large particle aggregation taking place at high concentration. Finally, 60 wt% samples only show a space-filling gel which displays in polarized-light microscopy a weakly birefringent texture due to frozen-in shear flows that occurred upon sample preparation (Figure 5).

Both the isotropic and nematic phases present a strong response to the application of external magnetic and electric fields. For example, the nematic phase displayed by the 30 and 40 wt% samples is easily aligned in only a few minutes by a rather weak magnetic field (0.5 T), as shown by polarized-light microscopy (Figure 7).

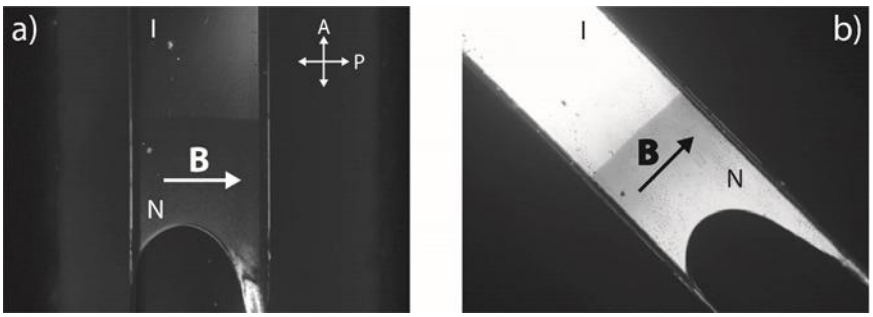

Figure 7. Application of a 0.5 T magnetic field B to the 30 wt% sample shown in Figure 6. The nematic phase is now uniformly planar and aligned along the magnetic field direction while the isotropic phase becomes birefringent due to the Cotton-Mouton effect.

This process results in the formation of a single domain of the nematic phase where all the nanodiscs are oriented with their normal parallel to the magnetic field, over macroscopic distances (i.e. several millimetres). The optical birefringence of the nematic phase can then be measured. The value obtained, $\Delta n = 0.011$, falls in between those of concentrated nematic suspensions of goethite nanorods ($\Delta n \approx 0.05$) and gibbsite platelets ($\Delta n \approx 5\times10\text{-}4$).[21] The magnetic field also had a small effect on the 50 wt% sample (Figure SI4), showing that the nanodiscs can move and reorient within the sediment. In contrast, the field had no effect at all on the 60 wt% gelled sample.

The nematic nature of the liquid-crystalline phase and its alignment by the magnetic field were confirmed by synchrotron small-angle X-ray scattering (SAXS) experiments. Indeed, the SAXS pattern of the 40 wt% sample (Figure 8a) only displays diffuse peaks (i.e. much broader than the experimental resolution) that are well oriented with respect to the magnetic field direction. At "wide" angles, a diffuse scattering peak, located at $q \approx 0.45$ nm-1, arises from some short-range positional order that is most probably due to particles stacking in short columns with a stacking period of ≈ 14 nm ($2\pi/0.45$ nm). At small angles, very close to the beamstop, diffuse scattering peaks located at $q \approx 0.09$ and 0.18 nm^{-1}, arise from the packing of these short, liquid-like, fluctuating columns in the plane perpendicular to the field, with an average inter-columnar spacing of ≈ 70 nm ($2\pi/0.09$ nm). Such spacings are in reasonable agreement with the particle dimensions and the volume fraction (i.e. the weight fraction divided by the particle density) of

the nematic phase. Therefore, at 40 wt%, the nematic phase of aqueous suspensions of CeF_3 nanodiscs has strong columnar local order and it is quite likely that gelation and aggregation pre-empt the formation of a columnar liquid-crystalline phase at higher concentration.

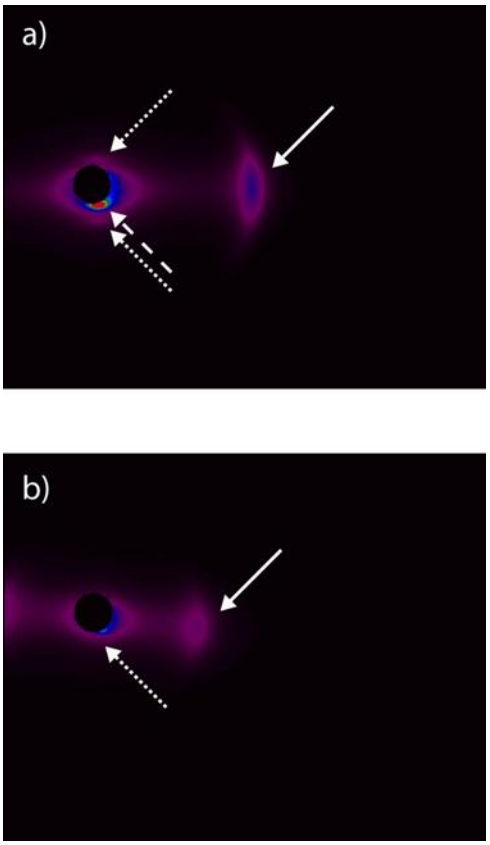

Figure 8. Anisotropic SAXS patterns of the nematic phase of suspensions of CeF_3 nanodiscs aligned in a 0.7 T horizontal magnetic field at a) 40 wt% and b) 30 wt% concentration. The solid arrow points to the diffuse scattering peak arising from short-range nanoparticle stacking. The dashed (resp. dotted) arrow points to the 1st order (resp. 2nd order) diffuse scattering peak arising from the short-range packing of the nanoparticle stacks in the plane perpendicular to their axes. (The 1st order diffuse peak can only be observed in Figure 8a and only on one side of the beamstop, as a red spot.)

Recording the SAXS pattern of an aligned sample of the nematic phase allows for the determination of its nematic order parameter, S, which is one of its important thermodynamic properties. S quantifies the strength of the orientational order and takes values between 0 (completely disordered phase) and 1 (perfect orientational order). S is classically inferred from the azimuthal scan of the scattered intensity along a circle centred on the origin and going through the "wide" angle diffuse peak.[21d, 22] The value obtained, $S = 0.90 \pm 0.05$, is very large; it contrasts with the values (~ 0.5 - 0.7) reported for common molecular liquid crystals used in display technology but it is actually typical of colloidal nematic phases.

The SAXS pattern (Figure 8b) of the 30 wt% sample is similar to that of the 40 wt% sample, except that, as expected, the columnar short-range order in the nematic phase is less pronounced and the typical distances between the particles (22 nm and 80 nm along and perpendicular to the director, respectively) are larger.

Altogether, the strong response to the magnetic field of the nematic phase of the suspensions of CeF_3 nanodiscs confirms their outstanding magnetic properties. Indeed, the paramagnetic behavior of the CeF_3 nanodiscs in suspension is further demonstrated by their slow migration to the regions of high field when they are submitted to a magnetic field gradient for long times (Figure S5). These observations are actually quite reminiscent of those made with suspensions of paramagnetic $GdPO_4$ nanorods.[23] Such phenomena illustrate the advantages of considering suspensions of mineral objects over organic ones to obtain original physical properties in soft condensed matter.

The isotropic phase of the colloidal dispersions of CeF_3 nanodiscs is also highly sensitive to the application of a magnetic field as it becomes birefringent, due to the partial orientation of the

nanodiscs by the field. This phenomenon, called Cotton-Mouton effect, is illustrated in Figure 9.[24]

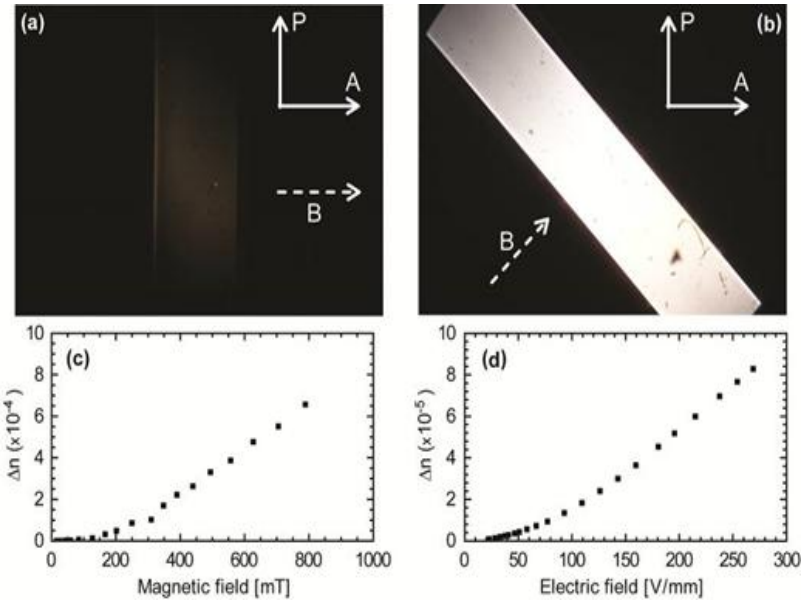

Figure 9. Orientational order induced by magnetic and electric fields in the isotropic phase of a colloidal suspension of CeF_3 nanodiscs (30 wt%) held in a 2 mm wide flat glass capillary. a) and b) microscopy images of the capillary observed between crossed polarizer and analyzer (white solid arrows, P and A) and submitted to a 0.8 T magnetic field (white dashed arrow); c) birefringence induced in the colloidal suspension versus magnetic field intensity; d) birefringence induced in the colloidal suspension versus electric field intensity.

The isotropic part of the 30 wt% sample submitted to a moderate magnetic field (0.8 T) becomes uniformly bright when the field lies at 45° with the directions of the polarizer and the analyzer whereas it appears completely dark when the field lies parallel either to the polarizer or analyzer directions (Figure 9a,b). The evolution of the sample birefringence (Δn) with magnetic field intensity (B), classically follows a quadratic dependence at small field but deviates from this behavior at large field (Figure 9c). The saturation of the birefringence, which corresponds to

perfect alignment of the nanodisc axis parallel to the field (S = 1), occurs at fields so large that it cannot be observed with our experimental setup. As expected, the birefringence disappears as soon as the field is removed. The susceptibility of this colloidal suspension to magnetic-field alignment can be quantified by the Cotton-Mouton coefficient $\Delta n/\phi B^2 = 0.028\ T^{-2}$ (where ϕ is the volume fraction), which is at least four orders of magnitude larger than the one obtained for suspensions of organic rods like the Tobacco Mosaic Virus and even larger than the recently reported colloidal suspension of $GdPO_4$ paramagnetic nanorods (0.013 T-2). However, it remains smaller than the huge value (0.55 T-2) obtained for suspensions of uncompensated antiferromagnetic α-FeOOH nanorods. [21a], [23], [25] A similar effect was studied by X-ray scattering on colloidal dispersions of $Ni(OH)_2$ nanoplatelets.[26]

The same kind of experiments was made by applying a high-frequency a.c. electric field to the isotropic part of the 30 wt% colloidal suspension of CeF_3 nanodiscs. The sample also turned birefringent as a result of the alignment of the particles in the electric field. The dependence of the birefringence on the field intensity shows a quadratic regime at small field that corresponds to the Kerr effect[27] of the suspension but it deviates from this regime at large field (Figure 9d), as also observed with suspensions of clay nanosheets and $LaPO_4$ nanorods.[28], [29] There again, perfect alignment of the particles could not be reached at the maximum field intensity provided by our setup. Interestingly, the dynamics of alignment and relaxation of the nanoparticles, when the electric field was switched on and off, showed typical response times of the order of 100 μs (see Supplementary Information for more details, Figure S6). Such fast response times make colloidal suspensions of CeF_3 nanodiscs interesting candidates for electro-optic applications.

The absorption spectrum of the colloidal suspensions is presented in Figure 12a (grey spectrum). Cerium fluoride usually exhibits five absorption bands that reflect the 5d excited configuration split by the crystal field (black spectrum). However, the absorption coefficient of CeF_3 is usually so high that it can only be measured on thin films.[30] Here, due to the presence of organic compounds in the colloidal dispersions, an additional absorption at wavelength smaller than 220 nm prevents the detection of the two highest energy bands located between 190 and 220 nm. We then only detect the three first bands located between 220 and 250 nm, which arise from the 4f-5d absorption and which are also observed for CeF_3 thin films. Diluted colloidal suspensions exhibit the well-known 4f-5d allowed electric dipole transition of trivalent cerium ions.

The emission properties of the CeF_3 nanoparticles suspensions in optical capillaries were measured with the three 30 wt%, 40 wt%, and 50 wt% samples after excitation at 250 nm (figure 10).

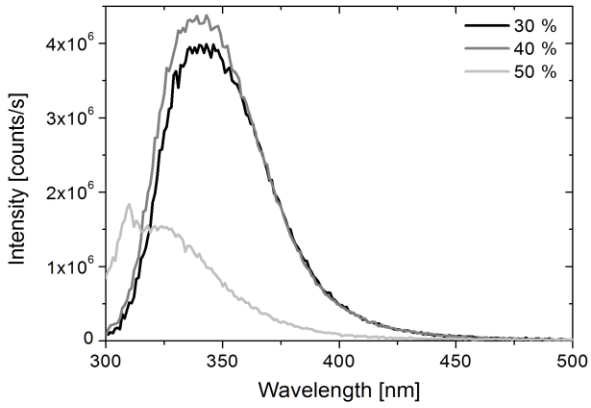

Figure 10. Emission intensity spectrum of three colloidal suspension at various concentrations (30%, 40% and 50% w/w) after excitation at 250 nm.

The low concentration (30 wt% and 40 wt%) samples showed a broad emission band with a maximum at 340 nm. This signal is consistent with the 5d-4f transition of Ce^{3+} ions in sites

perturbed by nearby surface defects. Interestingly, upon increasing weight fraction (50 wt% sample), the emission band was shifted down and showed two contributions at 310 nm and 325 nm and a much lower fluorescence intensity. This phenomenon could be attributed to an emission re-absorption process due to the high concentration of nanoparticles. The localization of the emission bands is in agreement with 5d-4f transitions of Ce^{3+} ions.

This spectroscopy study was extended by comparing the luminescence of the colloidal suspensions in capillaries with and without magnetic field (figure 11). Whatever the concentration of nanoparticles, the emission bands did not change in shape and position when the field was applied. However, the emission intensity of all samples strongly decreased, by a factor of 2-3. Thus, the magnetic field affects not only the orientation of the nanoparticles but also their fluorescence properties. We assume that the macroscopic alignment of the nanodiscs by the field enhances the non-radiative transfer or re-absorption of emission due to the reduced 5d–4f energy gap of Ce3+ in perturbed sites, leading to partial quenching of the emission properties of the particles. Indeed, the effect of the field on the 50 wt% sample is weaker than observed with the other two samples ie the lower concentrations, which is consistent with the fact that it has a lower effect on the particle alignment as previously described (Figure SI4).

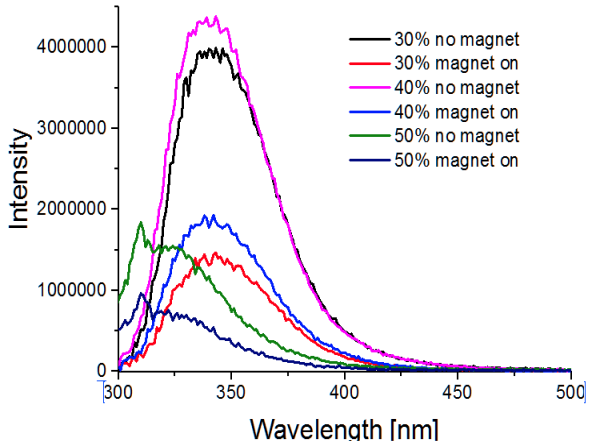

Figure 11. Fluorescence emission intensity of three samples 30%, 40% and 50% with or without magnetic field apply during measurement.

Finally, the scintillation properties of the CeF_3 particles were investigated. The main band detected at 300 nm under X-ray excitation (grey emission band on Figure 12a) corresponds to the main contribution of the Ce^{3+} regular site, as observed with CeF_3 single crystals. The discrepancy between the black and grey traces (standard sample and nanodiscs, respectively) is assigned to the remaining UV absorption, which artificially decreases the high-energy part of the emission spectrum of the nanodiscs. One may also observe a weak emission band at about 350 nm. As stated before, this emission is related to some surface states, as observed by Anderson et al.[31]

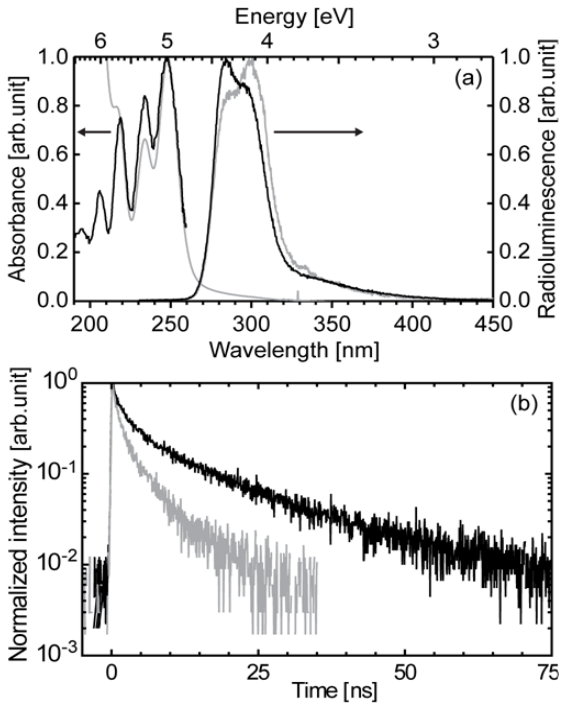

Figure 12. (a) Right-hand side: normalized luminescence spectrum of the CeF_3 nanoparticles (grey line) compared to that of a single crystal (black line). Left-hand side: absorption spectrum of a single crystal film (black line) from reference 43 compared to that of the nanoparticles (grey

line). (b) Normalized scintillation decay curve of the CeF_3 dried nanoparticles (grey line) compared to that of a single crystal (black line) measured under picosecond X-ray excitation.

In contrast to what was highlighted by Mishra et al. who used a molecular precursor approach, and by Zhu et al. who developed an ultrasonic method for the preparation of CeF_3 nanoparticles, we did not observe any broadening of the emission and absorption bands.[32] Band broadening is generally considered as the signature of an inhomogeneous crystal field. The absence of line broadening here actually confirms that the nanodiscs are perfectly crystallized, as already inferred from the TEM observations.

We also measured the scintillation decay under pulsed picosecond X-ray exposure (Figure 12b). Under high-energy excitation (x-ray tube set at 30kV), CeF_3 single crystals (black curve) exhibit an acceleration of the decay in its initial part, reflecting a weak scintillation quenching due to high concentration of charges during the energy relaxation process.[7],[33] In the case of the CeF_3 nanodiscs (grey curve), the decay rate is even faster. This reflects either the presence of surface quenchers such as dangling bonds or charge-confinement effects which may occur during the thermalization stage in the case of nanoparticles.[34] Thus, these systems exhibit very interesting scintillating properties compared to bulk CeF_3, particularly for applications requiring fast timing.

Conclusion

CeF_3 crystalline nanodiscs were synthesized using a simple and cheap protocol. Their functionalization with bisphosphonate ligands proved very efficient to transfer them in water to produce stable colloidal suspensions. In spite of the rather low aspect ratio (~ 6) of these nanodiscs, but in agreement with some numerical simulations, we found that the colloidal

suspensions spontaneously form a nematic liquid-crystalline phase at large volume fractions. This underlines the fact that, contrary to frequent belief, very large particle aspect ratios are not at all required for the nematic phase to appear, provided that large enough particle concentrations can be reached.

Thanks to the paramagnetic character of the nanodiscs, the nematic phase is easily and completely aligned by applying rather weak (~ 0.5) magnetic fields. This provides a simple, purely external, way of controlling the orientation of the nanodiscs in suspension. Moreover, very strong magneto-optic (Cotton-Mouton) and electro-optic (Kerr) effects were also observed in the isotropic phase. The fast time response of the latter makes it even possible to consider applications of these colloidal suspensions in electro-optic devices. In addition, the nanodiscs display very good scintillating properties which make them an easier and cheaper alternative to costly CeF3 single crystals. Processing these colloidal suspensions into functional scintillating materials could easily be achieved by spin-coating to prepare thin films or by polymerization of acrylamide to prepare bulk nanocomposites, as we recently demonstrated with other kinds of nanoparticles.[35]

ASSOCIATED CONTENT

(Word Style "TE_Supporting_Information"). **Supporting Information**. A listing of the contents of each file supplied as Supporting Information should be included. For instructions on what should be included in the Supporting Information as well as how to prepare this material for publications, refer to the journal's Instructions for Authors.

The following files are available free of charge.

brief description (file type, i.e., PDF)

brief description (file type, i.e., PDF)

AUTHOR INFORMATION

Corresponding Author

*(Word Style "FA_Corresponding_Author_Footnote"). * (Word Style "FA_Corresponding_Author_Footnote"). Give contact information for the author(s) to whom correspondence should be addressed.

Present Addresses

†If an author's address is different than the one given in the affiliation line, this information may be included here.

Author Contributions

The manuscript was written through contributions of all authors. All authors have given approval to the final version of the manuscript. ‡These authors contributed equally. (match statement to author names with a symbol)

ACKNOWLEDGMENT

We acknowledge the European Synchrotron Radiation Facility for provision of synchrotron radiation facilities, for the allocation of beamtime # SC4374, and we would like to thank Dr Sylvain Prévost for assistance in using beamline ID02.

REFERENCES

(Word Style “TF_References_Section”). References are placed at the end of the manuscript. Authors are responsible for the accuracy and completeness of all references. Examples of the recommended format for the various reference types can be found at http://pubs.acs.org/page/4authors/index.html. Detailed information on reference style can be found in *The ACS Style Guide,* available from Oxford Press.